BIOLOGICALLY INSPIRED MULTIFUNCTIONAL COMPOSITE PANEL WITH INTEGRATED CIRCULATORY SYSTEM FOR THERMAL CONTROL

A. D. Williams, M. E. Lyall, L. E. Underwood, and B. J. Arritt
Air Force Research Laboratory, Space Vehicles Directorate
3550 Aberdeen Ave, Kirtland AFB, NM 87117
afrl.rvsv@kirtland.af.mil

B. Taft
University of Wisconsin, Department of Mechanical Engineering
1513 University Avenue, Madison, WI 53706

SUMMARY

Multifunctional systems provide significant benefits at the systems level by increasing capability and decreasing mass. The focus of this effort is the development of a multifunctional structural panel that integrates a circulatory system directly into the face-sheet and structural ribs of an isogrid panel for greatly enhanced thermal control.

Keywords: multifunctional structures, isogrid panel, thermal control, spacecraft

INTRODUCTION

Satellite thermal control systems can be significantly enhanced via strap-on type systems, such as heat pipes, loop heat pipes, and pumped fluid loops. These systems improve thermal performance by improving heat transport efficiency and tight temperature control. , but add parasitic mass and reduce the usable volume of the satellite. The disadvantages are that they add parasitic mass, reduce the usable volume of the satellite, are expensive, and tend to be complex. In addition, they require power for temperature control.

Recently, there has been a surge in interest in biologically inspired or bio-mimetic structures where living organisms are used to provide guidance to improve overall performance of aerospace systems. In particular, the incorporation of a circulatory system to significantly improve the system physical properties, such as heat transfer, or enhance the system by adding a new capability, such as self-healing, is of interest. The key for these systems is to improve overall performance or add capability without increasing the overall mass of the system.

Because mass is an important parameter for aerospace systems, a key design factor for aerospace structures is the stiffness-to-weight ratio of the structure. For this reason, isogrid architectures are widely used in aerospace applications because they provide high stiffness and torsional rigidity while minimizing mass. By taking advantage of isogrid architectures, fluidic channels can be integrated into structural panels with minimal impact to the overall system structural efficiency and mass. The use of combined fluidic-structural systems has enormous potential for satellite thermal control,

and it will be shown that isogrid structures provide distinctive properties that allow for a symbiotic, biologically-inspired system. This paper will detail the design of a multifunctional composite isogrid panel that integrates fluidic channels into the structure for improved thermal control.

PANEL CONCEPT

Circulatory systems in biological organisms consist of three primary structures. The first is the main arterial system, which provides high fluid flow rates to the organs. The second is the capillary system, which distributes and controls the flow within the organ. The final is the heart, which is essentially a sophisticated pump. A system must consist of all of these elements and must coexist in a symbiotic relationship to be a truly biologically-inspired system. The distinctive properties of isogrid structures enable such a system; the ribs provide the necessary cross-sectional area for high flow rates and the face-sheets provide the surface area for the capillary distribution system. The concept is depicted in Fig. 1.

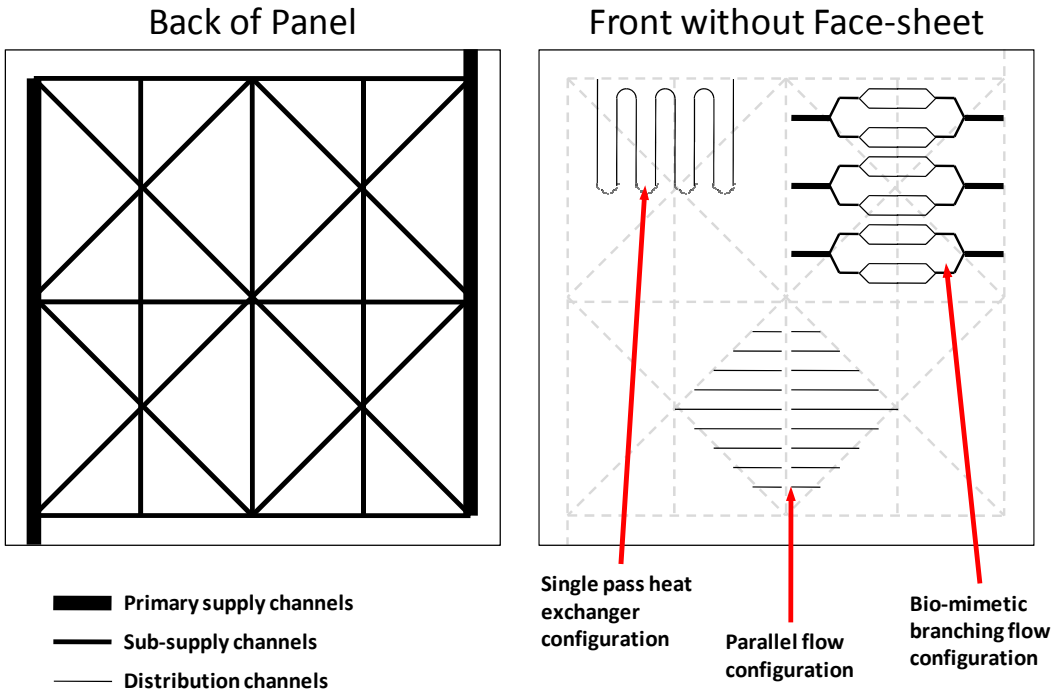

Figure 1: Schematic of the biologically inspired panel concept which integrates fluid channels into the rib structure and face-sheet

The system is designed such that the thermal control system can be varied to meet the needs of the components. The hollow ribs provide the primary fluid flow to the system, and the capillary distribution system provides the heat removal capability. To control the temperature of the subsystem, a passive, thermally-coupled valve controls the flow. When the component is too hot, the thermal valve opens and coolant passes from the arteries to the capillaries to cool the subsystem. The valves are thermally activated by the phase change expansion of paraffin and are thermally coupled to the component. The coolant flows out of the capillaries back into the main artery system where it flows into a radiator for cooling. The fluid is then pumped back into the arterial system.

When the subsystems are cool, the valve shuts off fluid flow so that the component can retain its heat thus limiting the heater power requirement for the system. Figure 2 shows a general schematic of the thermal subsystem.

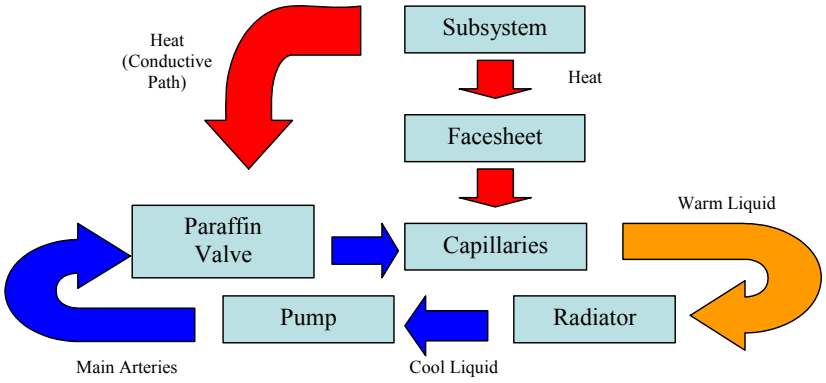

Figure 2: General thermal schematic for the symbiotic isogrid structure

The primary advantage of the isogrid architecture is the structural performance of the system after integration of the fluidic channels into the panel. Whereas the structural efficiency of other approaches degrades with the addition of fluidic channels, the performance of the isogrid structure does not[1]. To accommodate the fluid flow in the rib, the cross sectional area is increased, which increases the moment of inertia of the rib. The results are reductions in the bending and torsional stresses as well as an increase in the critical buckling load. Additionally, by incorporating smaller fluid channels under the surface of the panel face-sheet, the heat transfer capability of the panel surface can be significantly enhanced. The focus of this effort was to design a proof-of-concept panel that integrates the primary supply channels and the sub-supply channels into a composite isogrid panel. Future design iterations will focus on improving the adaptability and flexibility of the distribution channel system in the face-sheet.

From a thermal control standpoint, the most significant advantage of incorporating a circulatory system into the face-sheet of a satellite panel is modular, localized thermal management using efficient, forced-convection fluid loops. Additional benefit can be obtained by controlling the flow within the system. This can easily be accomplished with mature, active valve systems, but the requirements for power input, sensing, and control-system hardware for active systems reduce the symbiotic nature of the approach. Instead, a passive-reactive thermal valve provides a more symbiotic solution.

PANEL DESIGN AND OPTIMIZATION

The primary focus of this effort was to design and optimize the primary supply channels and the sub-supply channels to integrate them into the ribs of a composite isogrid panel without increasing the overall mass of the system. The fabrication of the face-sheet distribution channels is a straightforward process of machining the channels into the face-sheet and applying a top-sheet to seal the channels. Fig. 3 shows the basic geometric configuration of the panel, which is approximately 0.09 m^2.

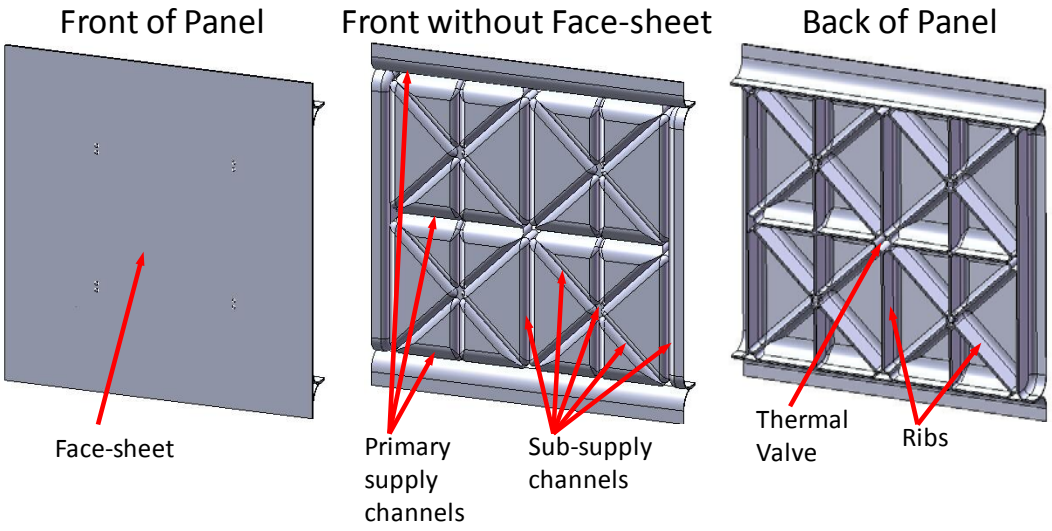

Figure 3: Front, front without face-sheet, and back views of the composite panel showing only the primary supply channels and sub-supply channels

Design Optimization Analysis Approach

Because of the fabrication approach used for the prototype panel, the basic channel geometry was set, which is shown in Fig. 4. However, the size of the channel could be adjusted by changing the radius of curvature of the branching arms of rib structure. The sub-supply channel size was determined by conducting a parameter study that examined the heat transfer, pressure drop, and face-sheet deflection for various channel sizes.

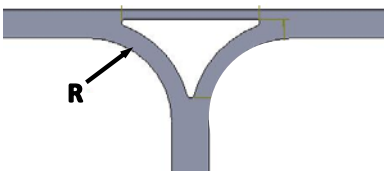

Figure 4: Schematic view of the face-sheet sub-supply channel cross section

Heat transfer:

To minimize the pumping power requirements for the system, the system flow rate was chosen to ensure laminar flow under all conditions. An internal flow is considered laminar for Reynolds numbers, Re, in the range of $Re < 2300$[2] and is determined using Eq. 1:

$$Re = \frac{\rho u D_h}{\mu} \tag{1}$$

where ρ is the density in kg/m^3, u is the velocity in m/s, D_h is the hydraulic diameter in m, and μ is the dynamic viscosity in N-s/m^2. For non-circular cross sections, D_h is given by Eq. 2:

$$D_h = \frac{4A}{p} \tag{2}$$

where A is the area of the cross section in m^2 and p is the perimeter of the cross section. The independent variable for the analysis was the radius of the channel fillet, R, and was varied over the range 2.54 mm $\leq$ R $\leq$ 12.70 mm in the parameter study. The resulting Reynolds number range was 55 < Re < 425.

To model the heat transfer to the channel, a constant heat flux boundary condition was assumed to correspond to a patch heater placed over the face-sheet channel area. In addition, fully developed flow for the entire length of the channel was assumed because the entry length was on the order of 2.5 cm for the Reynolds number range of interest[2]. It is also important to acknowledge that secondary flow effects would be present within the channel intersection points. The intersection points affected both the pressure drop analysis and the thermal analysis. For the pressure drop analysis, the flow through the intersections was treated as flow through either a tee or a 90° abrupt bend. For the thermal analysis, the primary effect was on the flow development as the fluid re-enters the channel. Again, fully developed flow was assumed for the entire length.

To compare the different cross sections, the heat load and outlet fluid temperature was kept constant for all cases. Assuming a constant heat transfer coefficient and realizing that the maximum fluid temperature occurs at the channel outlet, the maximum channel temperature was calculated based on the convection relation given by Eq. 3:

$$T_w = \frac{q}{hA_w} + T_{out} \tag{3}$$

where q is the heat added to the flow in W, h is the heat transfer coefficient in W/m^2-K, A_w is the wetted area of the channel, and T_{out} is the outlet temperature of the fluid. T_w in Eq. 3 represents the wall temperature directly adjacent to the fluid at the outlet of the face-sheet channel. For fully developed flow and a constant heat flux boundary condition, the fluid temperature rises linearly along the channel, and the temperature difference between the wall and fluid remains constant. The heat transfer coefficient, h, was calculated based on the non-dimensional Nusselt number, Nu, for internal fully developed laminar flow given by Eq. 4:

$$h = Nu\frac{k}{D_h} \tag{4}$$

where k is the thermal conductivity of the fluid in W/m-K. The cross section was assumed to be mostly triangular, and a Nu number of 3.11 was used[3].

Assuming constant material properties and using the known value of T_{out} and q, the mass flow rate in kg/s was calculated using the first law of thermodynamics, given by Eq. 5:

$$\dot{m} = \frac{q}{C_p(T_{out} - T_{in})} \tag{5}$$

where C_p is the specific heat in J/kg-K and T_{in} is the fluid temperature at the channel inlet. The mass flow rate was used to calculate the fluid velocity, which in turn was used to compute the pressure loss of the panel. Assuming an incompressible flow and

utilizing the conservation of mass principle, the fluid velocity was calculated in m/s according to Eq. 6:

$$u = \frac{\dot{m}}{\rho A} \tag{6}$$

Pressure drop:

To calculate the overall pressure loss of the panel, the fluid velocity was calculated for the sub-supply channels. Because of the large cross-sectional area and corresponding low velocity, the losses were ignored in the primary supply channels.

The pressure loss was computed based on both major and minor losses. The major losses accounted for the losses in the long straight sections of the channel. The minor losses were used to account for the pressure loss in the bends and discontinuities of the channel. The major losses were calculated according to Eq. 7[4]:

$$h_{maj} = \frac{1}{2} f u^2 \frac{L}{D_h} \tag{7}$$

where f is the dimensionless friction factor and L is the length of the channel in m for which the loss was being computed. Because the flow for all conditions in this analysis was laminar, the friction factor was independent of surface condition and was computed according to Eq. 8[4]:

$$f = \frac{53}{Re} \tag{8}$$

The minor losses due to abrupt discontinuities were calculated according to Eq. 9:

$$h_{min} = \frac{1}{2} K u^2 \tag{9}$$

where K represents a non-dimensional loss factor. The loss factor K was available in the literature based on experimental data[4]. However, the losses in the serpentine face-sheet channel due to gradual bends were computed by Eq. 10:

$$h_{min} = \frac{1}{2} f u^2 \frac{L_e}{D_h} \tag{10}$$

where L_e represents an equivalent length of channel. The L_e/D_h ratios were also obtained from experimental data in the literature[4]. The overall pressure loss of the panel was calculated according to Eq. 11:

$$\Delta P_{loss} = \rho \sum (h_{min} + h_{maj}) \tag{11}$$

where ΔP_{loss} is the overall pressure loss of the panel in Pa.

Face-sheet deflection:

The primary structural requirement of the channel is to resist deflection caused by the fluid pressure. Because the geometry of the curved walls naturally resist deflection, the primary concern was the deflection of the face-sheet. Minimizing face-sheet deflection was also important to provide a flush mounting surface for the components. To

calculate the face-sheet deflection, the problem was simplified to a simple one-dimensional beam bending problem with uniform load and fixed support boundary conditions. The maximum deflection at the center of the span was calculated with Eq. 12[5].

$$y_{max} = \frac{wl^4}{384EI} \tag{12}$$

where w is the load in N/m, l is the length of the span in m, E is modulus of elasticity in Pa, and I is the second moment of area in m^4.

Design Optimization Results and Discussion

To determine the optimized radius for the channel geometry, each of the design parameters was normalized according to Eq. 13 for easier comparison.

$$x^* = \frac{x_{value} - x_{min}}{x_{max} - x_{min}} \tag{13}$$

The results for each parameter are presented in Fig. 5 for a heat input of 70 W and a flow rate of 50 mL/min. As shown, both the pressure and thermal performance of the panel improved with increasing cross sectional area on a path of diminishing returns. The trade-off was an increase in face-sheet deflection as the span increased.

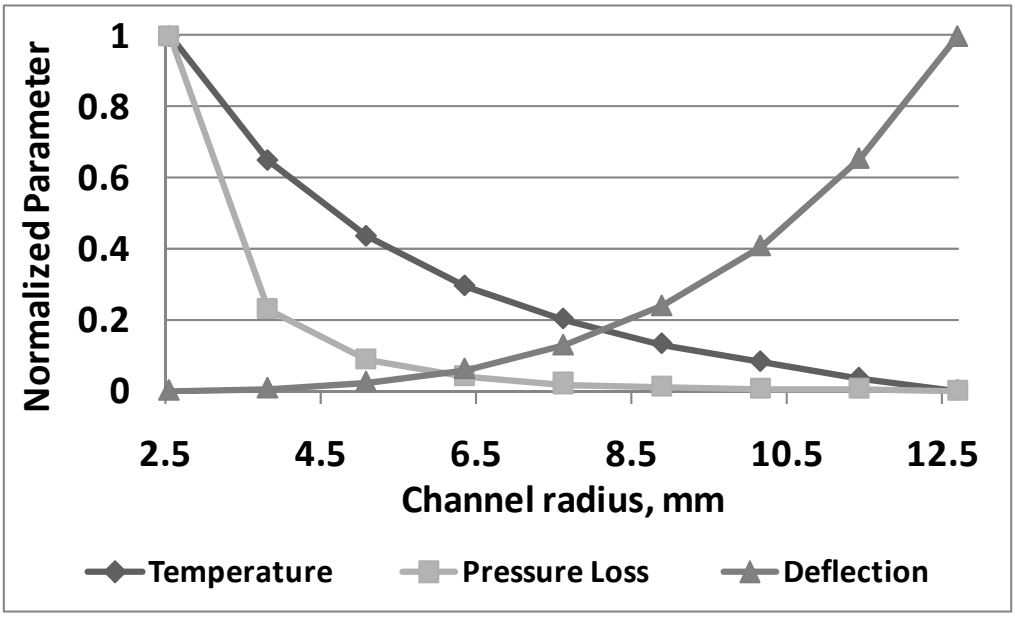

Figure 5: Plot of the normalized temperature, pressure loss, and face-sheet deflection of the thermal-structural panel

To summarize the performance analysis, it was desired to achieve the optimal performance based on the assumed channel geometry. It is for this reason that a channel radius of 7.6 mm was chosen. However, it is also worth noting that the purpose of this study was not to optimize in terms of heat transfer augmentation but to integrate cooling channels within a composite isogrid structural architecture. The parameter study discussed in this section was aimed at selecting the most appropriate cross section, which can easily be prototyped.

VALVE DESIGN

In addition to the panel design, an important aspect of the concept was the design of the passive-reactive thermal valve. The focus of this design effort was to design for both functionality and maintainability to facilitate experiments in the lab. Although not drawn to scale, Fig. 6 presents a schematic representation of the valve layout in the actuated, or open, position. The valve utilizes the expansion properties of paraffin wax as it melts to open the valve and the spring force of Bellville washers to close the valve as the paraffin solidifies.

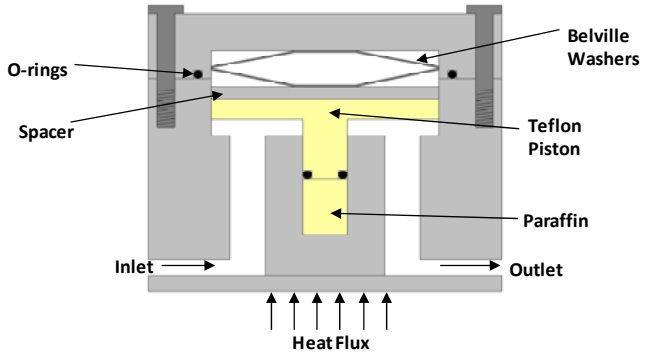

Figure 6: Schematic cross-section view of the passive-reactive valve

Nonadecane ($C_{19}H_{40}$) paraffin was chosen because its phase change begins at 295 K, which is consistent with the normal operating temperature range for most satellite bus components. Nonadecane begins undergoing solid-solid transitions at 295 K and completes the solid-liquid transition at 304 K[6]. During this transitioning process, it expands approximately 11.8% by volume. Although not clear in the schematic view, the paraffin chamber was cylindrical and limited motion to one axis. This resulted in an 11.8% linear actuation distance based on the overall height of the paraffin pellet. The paraffin chamber was sized to provide adequate flow through the valve.

Belville washers, which provide high spring constants for small displacements, provided the return force to close the valve. Coil springs were examined, but the available spring constants were too low for the lengths required for this application. As shown in Fig. 6, two washers were stacked end to end to achieve the desired displacement and return force. The spring chamber was sized to create a preload on the piston to ensure proper sealing. Teflon was chosen as the piston material to resist sticking. For the overall paraffin phase change process, the spring force, F_s, was designed to vary within the range of $71 \leq F_s \leq 245$ N.

In designing the paraffin chamber, two competing factors were considered. First, to minimize the valve actuation time, the pellet diameter must be small. If the phase change time was too long, the component could overheat. Second, the cylinder diameter had to be large enough to accommodate off-the-shelf o-ring sizes, which effectively set the minimum value for the paraffin chamber diameter. Based on the latter aspect, the cylinder diameter was set at 5.8 mm.

To verify the acceptability of the proposed diameter, a simplified phase-change analysis was conducted to determine the melt time and resulting interface boundary temperature. The system was modeled as a one-dimensional infinite solid to provide a conservative estimate. The actual paraffin pellet will melt much faster because heat is applied to all

sides of the cylinder as well as the base of the valve. The melting process of the analysis is depicted in Fig. 7 and assumes the material is initially at the melt temperature, T_m. As heat is applied to the boundary, the location of the solid-liquid interface, s(t), moves with time and the temperature of the liquid rises. This process is stated mathematically in Eqs. 14a-d[7]:

$$\frac{\partial^2 T(x,t)}{\partial x^2} = \frac{1}{\alpha}\frac{\partial T(x,t)}{\partial t} \qquad 0 < x < s(t), t > 0 \qquad (14a)$$

$$-k\frac{\partial T}{\partial x} = q'' \qquad 0 = x, t > 0 \qquad (14b)$$

$$T = T_m \qquad x = s(t), t > 0 \qquad (14c)$$

$$-k\frac{\partial T}{\partial x} = \rho L\frac{ds(t)}{dt} \qquad x = s(t), t > 0 \qquad (14d)$$

where α, ρ, and L are the thermal diffusivity, density, and latent heat of fusion in m^2/s, kg/m^3, and J/kg respectively for nonadecane. Note that the temperature profile defined by these equations is for the liquid zone.

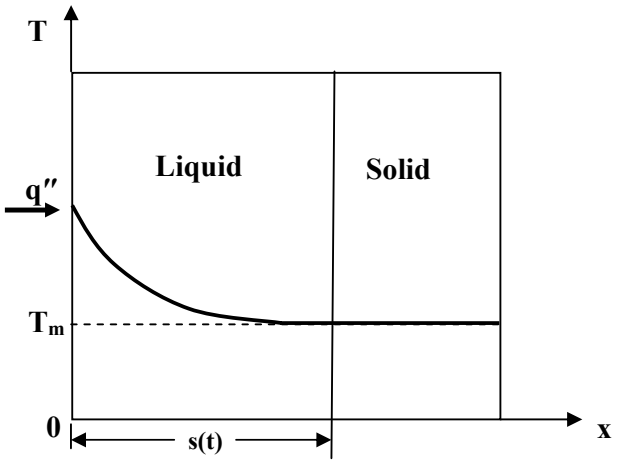

Figure 7: Diagram of the melting process

Equations 14a-d were solved by assuming a linear temperature profile and using the integral method for approximating partial differential equations[7]. The temperature profile as a function of distance and time for a semi-infinite solid with a constant surface heat flux condition is given by Eq. 15:

$$T(x,t) = T_m - \frac{q''(x - s(t))}{k} \qquad (15)$$

The solid-liquid interface location is given by Eq. 16[7]:

$$s(t) = \frac{1}{2}\left[\left(\frac{2L\rho\alpha}{q''}\right)^2 + 8\alpha t\right]^{1/2} - \rho L\frac{\alpha}{q''} \qquad (16)$$

For a typical component heat flux of 500 W/m^2, a melt time of 14 minutes was required. However, the more important parameter was the increase in surface temperature at the heat flux boundary. The resulting temperature difference was 4 K. It is also important to note that the melt time varies indirectly with heat flux, but the temperature difference remains essentially constant. As a result, the valve responds in accordance with the cooling needs of the system. Based on the simplified analysis, it appears that the response of the valve is compatible with typical spacecraft thermal time constants. Future experimental measurements are planned to verify the numerical predictions and so validate this symbiotic approach.

CONCLUSIONS

The primary focus of the effort was to design a composite, biologically inspired structural panel that integrated a circulatory, or pumped fluid system, into an isogrid structure to significantly improve cooling performance. The fluid supply channels, which mimic arteries and veins, were integrated into the rib structure of the panel, and the fluid distribution channels, which mimic the capillaries within the organs, were integrated into the face-sheet of the panel. A prototype panel and a passive-reactive thermal valve were designed, and an optimized channel configuration was identified that included thermal, pumping, and fabrication issues. The channel configuration can best be summarized as an isosceles triangle where the equal length sides have been replaced with arcs with a radius of 7.6 mm; this arc length offered the best combination of thermal, pressure loss, and structural performance.

References

1. Williams, A. D., Arrit, B., Millan, D., Taft, B., and Nieuwdoop, A., "Biologically Inspired Thermal-Structural Satellite Panels," 48th AIAA/ASME/ASCE/AHS/ASC Structures, Structural Dynamics, and Materials Conference, April 2007
2. Bejan, A., Convection Heat Transfer, 3rd ed., John Wiley & Sons, New Jersey, 2004, Chapter 3.
3. Incropera, F. P., and DeWitt, D. P., *Fundamentals of Heat and Mass Transfer*, 4th ed., John Wiley & Sons, New York, 1996, Chapters 5 and 8.
4. Fox, R. W., and McDonald, A. T., *Introduction to Fluid Mechanics*, 5th ed., John Wiley & Sons, New York, 1998, Chapter 8.
5. Shigley J. E., and Mischke C. R., *Mechanical Engineering Design*, 6th ed., McGraw-Hill, New York, 2001, pg 1186.
6. Huang, D., Sindee, L. S., and Mckenna, G. B., "Chain Length Dependence of the Thermodynamic Properties of Linear and Cyclic Alkanes and Polymers," The Journal of Chemical Physics [online journal], Vol 122, No. 084907, Paper 1, URL: http://link.aip.org/link/?JCPSA6/122/084907/1
7. Özişik, M. N., *Heat Conduction*, 2nd ed., John Wiley & Sons, New York, 1993, Chapter 11.